PERGAMON

International Journal of Solids and Structures 39 (2002) 5799–5812

INTERNATIONAL JOURNAL OF SOLIDS and STRUCTURES

www.elsevier.com/locate/ijsolstr

Computational studies on high-stiffness, high-damping SiC–InSn particulate reinforced composites

Hyung Joo Kim [a], Colby C. Swan [b,*], Roderic S. Lakes [c]

[a] *Mechanical Engineering, Center for Computer-Aided Design, The University of Iowa, Iowa City, IA, USA*
[b] *Department of Civil and Environmental Engineering, Center for Computer-Aided Design, The University of Iowa, 52242 Iowa City, IA, USA*
[c] *Engineering Physics, The University of Wisconsin, Madison, WI, USA*

Received 11 October 2001; accepted 20 May 2002

Abstract

With the objective of achieving composite material systems that feature high stiffness and high mechanical damping, consideration is given here to unit cell analysis of particulate composites with high volume fraction of inclusions. Effective elastic properties of the composite are computed with computational homogenization based on unit cell analysis. The correspondence principle together with the viscoelastic properties of the indium–tin eutectic matrix are then used to compute the effective viscoelastic properties of the composite. Comparison is made with parallel experiments upon composites with an indium–tin eutectic matrix and high volume fractions of silicon-carbide reinforcement. The analytical techniques indicate that combinations of relatively high stiffness and high damping can be achieved in particulate composites with high SiC volume fractions. Based on analysis, the tradeoffs between stiffness and damping characteristics are assessed by changing the volume fraction, size, packing, and gradation of the particulate reinforcement phases. Practical considerations associated with realization of such composites based on the surface energy between the SiC and the InSn are discussed.

Keywords: Viscoelastic; Damping; Effective properties; Homogenization; Particulate composites

1. Introduction

1.1. Motivation

In many structural applications it is desired to use materials that are not only stiff and strong, but also that have the ability to damp mechanical vibrations. Since elastic moduli measure the stiffness of the material and $\tan\delta$ the damping, the product of the two is a useful figure of merit that combines both properties. Hence for shearing vibrations, the product $G\tan\delta$ is useful, whereas for bending and/or

* Corresponding author. Tel.: +1-319-335-5831; fax: +1-319-335-5660.
E-mail address: colby-swan@uiowa.edu (C.C. Swan).

0020-7683/02/$ - see front matter
PII: S0020-7683(02)00404-3

extensional vibrations $E \tan \delta$ would be used. For polymer matrix materials, it is difficult to achieve values of $E \tan \delta$ in excess of 0.6 GPa. Furthermore, polymers suffer from temperature sensitivity, flammability, and have a narrow effective frequency range. For these reasons, viscoelastic metallic materials systems are sought here that have both high stiffness and high damping. Although the study of viscoelastic materials has been conducted for some years, attempts at the intentional design of materials with high loss based on known mechanisms is relatively recent, and the field is embryonic at this stage.

1.2. Rationale for the current approach

In the current effort, a high-damping but low-stiffness metallic matrix material and a high-stiffness but low-damping reinforcement phase are combined to seek high stiffness and high damping. Particulate composites with a high volume fraction of particulate reinforcement are one fairly simple means of achieving this objective. A number of analytical micromechanics frameworks for predicting effective moduli (Christensen, 1979; Tandon and Weng, 1986; Ju and Chen, 1994) and strengths (Ju and Sun, 2001) of particle-reinforced composites with generalized spheroidal or ellipsoidal inclusions have been successfully developed and applied, but most have difficulty addressing strong particle–particle interactions, and are thus limited to particle volume fractions less than about 50%. Arbitrarily high concentrations of coated spherical inclusions can be dealt with analytically for the bulk and shear moduli (Hashin, 1962) using a hierarchical coated sphere approach in which the composite is filled with inclusions of different size. This morphology attains the Hashin-Shtrikman upper bounds for the bulk and shear moduli when the coating is the stiffer phase, and it realizes the lower bound on these moduli if the coating is the less-stiff phase with the particle made of the stiffer phase. Similarly, a hierarchical laminate (Francfort and Murat, 1986; Milton, 1986) exactly attains the Hashin-Shtrikman bounds for the shear modulus. These hierarchical particulate and laminate morphologies are difficult to achieve in real materials, since ideally, structure is required at all levels of scale. To examine more realistic inclusion morphologies which lend themselves to high volume fraction, we here consider tight regular packing of particulate composites with two different sizes of reinforcement.

Since such composites are difficult to model analytically, a unit-cell homogenization approach framework is adopted here. Such techniques can be used with either finite element methods (Swan, 1994; Swan and Kosaka, 1997; Guedes and Kikuchi, 1991), or spectral methods (Dumont and Lebon, 1996; Michel et al., 2001). Since finite element methods tend to be more robust than spectral techniques, and since they do not suffer from convergence difficulties, they are used in the present study. Such unit-cell approaches are often used to model both elastic and inelastic behavior within composites.

For the micromechanical analysis portion of this work, both the metallic matrix and the particulate reinforcement phase are treated as linearly elastic solids. Once the effective elastic properties of the composite are obtained for different reinforcing sizes, shapes and arrangements, the correspondence principle is used to generate effective viscoelastic properties of the composites. Data at a single frequency (1 Hz) are chosen for input. At other frequencies both the stiffness and damping of the compliant damping phase will be different.

1.3. Material selection considerations

An important consideration in the design of high-stiffness, high-damping metallic composites is that of selecting appropriate matrix and reinforcing materials. In this work, attention is confined to a high-damping matrix and stiff inclusions. Consideration of alternatives based on high damping inclusion phases like lead metaniobate of moderate stiffness were considered in (Goodman, 1953; Berlincourt et al., 1964; Lee and Lakes, 2001). An experimental proof of concept for a high-damping matrix and high stiffness inclusions was presented in Brodt and Lakes (1995) for laminates consisting of InSn alloy and tungsten. The combination of

stiffness and loss (the product $E\tan\delta$) of this composite exceeds that of well-known materials such as polymer layers. Tungsten was chosen since it is stiff, albeit quite heavy and expensive. Cast indium tin alloy was chosen since it exhibits high damping properties for a metal (Brodt and Lakes, 1995; Lakes and Quackenbush, 1996). Alternative constituents were also sought to facilitate practical application of these concepts.

Cast InSn was again selected for usage in this study. Alternate metal matrix phases and processing modalities might also have been considered. For example modification by superplastic transformation, specifically by rolling, gives rise to enhanced damping in a eutectic PbSn alloy. Damping (Buechner et al., 1999) of superplastic eutectic Pb–Sn is considerably higher than that of cast Pb–Sn, solder wire, and eutectic Pb–Sn. Quenching (rapid cooling) of high damping metals (Dooris et al., 1999) such as InSn also increases the damping, but much of the effect is lost as a result of aging over a period of about a year. Plastic deformation also increases the damping of Sn and InSn.

SiC particulate powder is promising as a stiff alternative to tungsten. It is stiff but inexpensive and lightweight, with a Young's modulus of 420–450 GPa (Lloyd, 1994) compared with 400 GPa for tungsten, 200 GPa for steel, and 70 GPa for aluminum and its alloys. SiC has a density $\rho = 3.2$ g/cm^3, much lower than that of tungsten, 19 g/cm^3, and is comparable to that of aluminum, 2.7 g/cm^3. Experimental studies (Ludwigson et al., in press) of particulate SiC–InSn show composite shear modulus to be almost a factor two greater than matrix for 40% volume content of particles and a factor of four greater than that of matrix for 60% volume content. Damping was similar to that of the InSn matrix over a significant part of the frequency range. If the high damping phase were stiffer, a smaller concentration of stiff particles would suffice (Brodt and Lakes, 1995).

2. Analytical modeling

2.1. Unit cell analysis of particulate composites

2.1.1. Spherical and cubical inclusions and their arrangements

The objective of this analysis is to find arrangements of discrete particulate reinforcement that achieve high-volume fractions, and to compute the homogenized stiffness properties associated with such composites. If we first consider a composite with only a single size of inclusions, and that these inclusions are arranged in a face centered cubic (FCC) pattern a reinforcing volume fraction of up to about 70% can be achieved. With two different sizes of reinforcement spheres ($r_1 = 1$; $r_2 = 0.414$), up to about 80% volume fraction of reinforcement can be achieved (Fig. 1). To achieve particulate reinforcing volume fractions approaching the vicinity of 95%, a fairly broad spectrum of particle sizes would be needed, making the unit cell analysis more computationally expensive, and the composites themselves more difficult to fabricate. To overcome saturation of volume fraction when dealing with spherical inclusions, composites with cubical inclusions have also been considered. The arrangement for such inclusions are taken to follow a simple cubic (SC) pattern shown in Fig. 2.

2.1.2. The unit cell problem

The particulate composites under consideration here are assumed for simplicity to exhibit periodic microstructures in that a single wavelength sub-domain forms a unit cell $\Omega_s = \Pi_{i=1}^{3}]0, \lambda_i[$, where λ_i are the dimensions of a specific composite's unit cell. Regions of the structural domain Ω_b are formed by repetition of the composite's unit cell Ω_s. Material points in an undeformed unit cell Ω_s are referenced by local material scale coordinates $\mathbf{X}$, while the spatial material scale coordinates $\mathbf{x}$ locate material points in a deformed cell. Similarly, the Lagrangian and spatial macroscale coordinates of a point in the larger domain

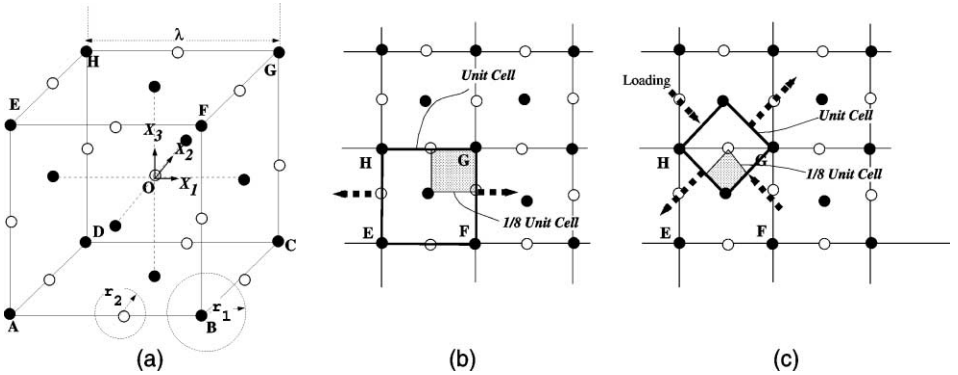

Fig. 1. Regular, periodic arrangement of spherical reinforcing particles of two different sizes within a composite: (a) inclusion arrangements; (b) unit-cell model for tension test; (c) unit-cell model for shear test.

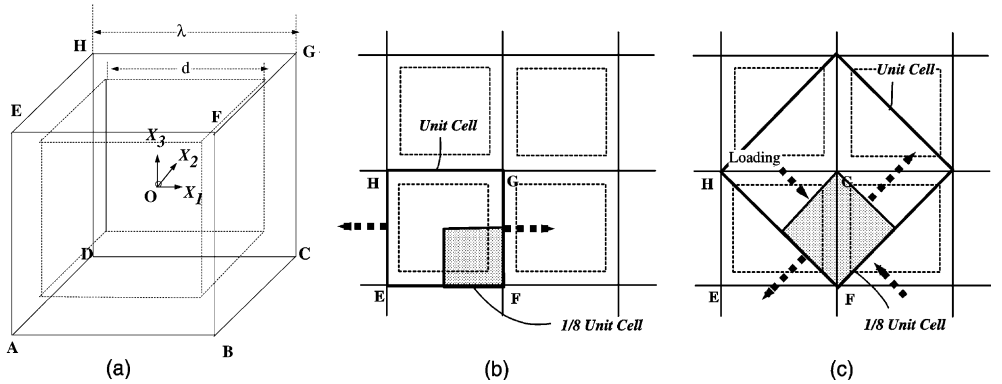

Fig. 2. Unit cell associated with periodic, square-packed arrangement of cubical inclusions: (a) inclusion arrangements; (b) unit-cell model for tension test; (c) unit-cell model for shear test.

Ω_b are denoted by $\mathbf{Y}$ and $\mathbf{y}$. The undeformed and deformed locations of a material point are related by displacement vectors $\mathbf{u}$ such that

$$\mathbf{x} = \mathbf{X} + \mathbf{u}(\mathbf{X}) \text{ material scale}; \quad \mathbf{y} = \mathbf{Y} + \mathbf{u}(\mathbf{Y}) \text{ macroscale}. \tag{2.1}$$

Material scale coordinates $\mathbf{X}$ and $\boldsymbol{x}$ are used in solving unit cell homogenization problems, whereas macroscale coordinates $\mathbf{Y}$ and $\boldsymbol{y}$ are used in solving structural analysis problems with the effective medium approximation. At the material scale, and at the macroscale, the respective deformation gradients are defined as follows:

$$\mathbf{F}(\mathbf{X}) = \frac{\partial \mathbf{x}}{\partial \mathbf{X}}; \quad \mathbf{\Phi}(\mathbf{Y}) = \frac{\partial \mathbf{y}}{\partial \mathbf{Y}}. \tag{2.2}$$

If the length scale of variation l associated with deformation $\mathbf{\Phi}$ in a composite structural element Ω_b is much larger than the wavelengths of the material microstructure ($l/\|\boldsymbol{\lambda}\| \gg 1$) then the deformation and stress fields will be λ-periodic on the material scale such that

$$\mathbf{F}(X_I) = \mathbf{F}(X_I + n\lambda_I), \quad \boldsymbol{\sigma}(X_I) = \boldsymbol{\sigma}(X_I + n\lambda_I), \quad I = 1, 2, 3, \tag{2.3}$$

where n is a small, but otherwise arbitrary integer, $\boldsymbol{\sigma}(\mathbf{X})$ is the local Piola–Kirchoff stress tensor, and $\mathbf{F}(\mathbf{X})$ is the local deformation gradient. Periodicity of one field (deformation or stress) typically assures periodicity of the other. The periodicity of the stress and deformation field on the material scale suggests that they admit additive decompositions into macroscopic contributions $(\mathbf{S}, \boldsymbol{\Phi})$, which are constant on the micro-scale, and purely oscillatory contributions $[\boldsymbol{\sigma}^*(\mathbf{X}), \mathbf{F}^*(\mathbf{X})]$, which can vary quite significantly on the unit cell length scale:

$$\boldsymbol{\sigma}(\mathbf{X}) = \mathbf{S} + \boldsymbol{\sigma}^*(\mathbf{X}), \quad \mathbf{F}(\mathbf{X}) = \boldsymbol{\Phi} + \mathbf{F}^*(\mathbf{X}). \tag{2.4}$$

The homogenized macroscopic tensors $(\mathbf{S}, \boldsymbol{\Phi})$ are defined as volume averages of $(\boldsymbol{\sigma}, \mathbf{F})$ over the undeformed unit cell, and have the mathematical definitions:

$$\mathbf{S} = \langle \boldsymbol{\sigma} \rangle = \frac{1}{V} \int_{\Omega_s} \boldsymbol{\sigma} \, \mathrm{d}\Omega_s, \quad \boldsymbol{\Phi} = \langle \mathbf{F} \rangle = \frac{1}{V} \int_{\Omega_s} \mathbf{F} \, \mathrm{d}\Omega_s, \tag{2.5}$$

where V is the initial volume of the unit cell $\overline{\Omega}_s$. Combining (2.4) and (2.5) it can be shown that

$$\langle \boldsymbol{\sigma}^* \rangle = \mathbf{0}, \quad \langle \mathbf{F}^* \rangle = \mathbf{0}. \tag{2.6}$$

With regard to the constant-periodic decomposition of the deformation field, it can also be shown by integrating (2.4, second term) that the displacement field over an individual unit cell must admit a linear-periodic decomposition:

$$\mathbf{u}(\mathbf{X}) = [\boldsymbol{\Phi} - \mathbf{1}] \cdot \mathbf{X} + \mathbf{u}^*_{\mathrm{per}}(\mathbf{X}), \tag{2.7}$$

where any constant or rigid body contributions to the displacement field $\mathbf{u}$ are eliminated by proper restraints on the unit cell domain, and imposing $\boldsymbol{\Phi} = \mathbf{R} \cdot \mathbf{U}$, where $\mathbf{R}$ is a rotation operator, and $\mathbf{U}$ is the right stretch tensor. The periodic displacement field contribution $\mathbf{u}^*_{\mathrm{per}}(\mathbf{X})$ permits a heterogeneous (non-uniform) deformation field within the unit cell domain $\overline{\Omega}_s$, satisfying local stress equilibrium $\sigma_{IJ,I} = 0$.

2.1.3. The effective elastic stiffness tensor $\boldsymbol{C}$

The deformation-controlled homogenization problem involves imposing macroscopic deformation $\boldsymbol{\Phi}$ (or imposing $\mathbf{u} = [\boldsymbol{\Phi} - \mathbf{1}] \cdot \mathbf{X}$) on the cell of a composite and computing the resulting periodic minimal energy displacement field $\mathbf{u}^* : \overline{\Omega}_s \Rightarrow \Re^3$ satisfying the equilibrium equation ($\nabla \cdot \boldsymbol{\sigma} = 0$ on $\overline{\Omega}_s$). From the equilibrium local displacement field $\mathbf{u}(\mathbf{X})$, strain–displacement relations, and constitutive behaviors of the materials in the composites, the corresponding stress field $\boldsymbol{\sigma}(\mathbf{X})$ and its macroscopic counterpart $\mathbf{S}$ can be computed. For the special case of a composite material being comprised of linearly elastic and perfectly bonded constituents, the functional form of the effective constitutive behavior for the composite will necessarily be that of linear, anisotropic elasticity. Using deformation-controlled homogenization, the components of a composite's linearized anisotropic stiffness tensor $\mathbf{C}$ can be calculated straightforwardly as follows: given a state of macroscopic deformation $\boldsymbol{\Phi}$ imposed on the unit cell. The associated macroscopic strain (Green–Lagrange) is computed as

$$E_{KL} = \frac{1}{2}[\Phi_{kK}\Phi_{kL} - \delta_{KL}]. \tag{2.8}$$

The local equilibrium equation $\nabla \cdot \boldsymbol{\sigma}^{(KL)} = \mathbf{0}, \forall \mathbf{X} \in \overline{\Omega}_s$ is then solved (subject to periodic boundary conditions) for the unknown part of the material-scale displacement field $[\mathbf{u}^*(\mathbf{X})]^{(KL)}$ on the domain of the unit cell $\overline{\Omega}_s$. In solving a weak form of the local equilibrium state equation over $\overline{\Omega}_s$ via the finite element method, the local strain and stress fields are explicitly computed. By the *average stress theorem* for composites subjected to macroscopically homogeneous deformation loading Φ_{kK}, the macroscopic stress tensor $S_{IJ}^{(kK)}$ corresponding to the applied macroscopic strain E_{KL} is simply the volume average of the local stress field.

$$S_{IJ}^{(KL)} = \frac{1}{V}\int_{\Omega_s} \sigma_{IJ}^{(KL)}\,\mathrm{d}\Omega_s. \tag{2.9}$$

Accordingly, by solving the unit cell problem for all appropriate and necessary permutations of the K and L indices of the macrostrain tensor $\mathbf{E}$. The coefficients of the effective medium elastic stiffness tensor for the composite are simply

$$C_{IJKL} = \begin{cases} \dfrac{S_{IJ}^{(KL)}}{E_{KL}} & \text{if } K = L \\ \dfrac{S_{IJ}^{(KL)}}{2E_{KL}} & \text{if } K \neq L \end{cases}, \tag{2.10}$$

where there is no sum on repeated indices in the denominator.

2.1.4. Symmetry considerations and FEM solution of unit cell problems

For the class of composite materials under consideration, the unit cells feature three planes of symmetry. When the deformation loading applied to the unit cell is symmetric with respect to these planes of symmetry, then the inhomogeneous periodic displacements $\mathbf{u}^*$ will vanish on the boundaries of the unit cell. In these cases, one can solve the material scale analysis problem on only one-quarter or one-eighth of the full unit cell as is shown in Figs. 1 and 2. The actual meshes used in these computations (Fig. 3) were generated using the algorithms described in Kim and Swan (in press, 2002). Ten-noded tri-quadratic tetrahedral continuum elements comprise the mesh. The FEM code used to solve the analysis problems is described in Swan (2001). All reported results based on finite element solutions of unit cell analysis problems were verified to be converged with mesh refinement.

2.2. Effective viscoelastic properties by the correspondence principle

Behavior of viscoelastic composites is predicted by the elastic–viscoelastic correspondence principle (Christensen, 1969; Hashin, 1970). The correspondence principle allows one to obtain a quasi-static solution for a boundary value problem for a viscoelastic material given a quasi-static solution for an elastic material. By this means, the relationship between constituent and composite elastic properties are converted to a steady state harmonic viscoelastic relation by replacing the real shear moduli G by complex moduli $G^*(\mathrm{i}\omega)$ or G^*, in which ω is the angular frequency of the harmonic loading. The fundamental assumptions

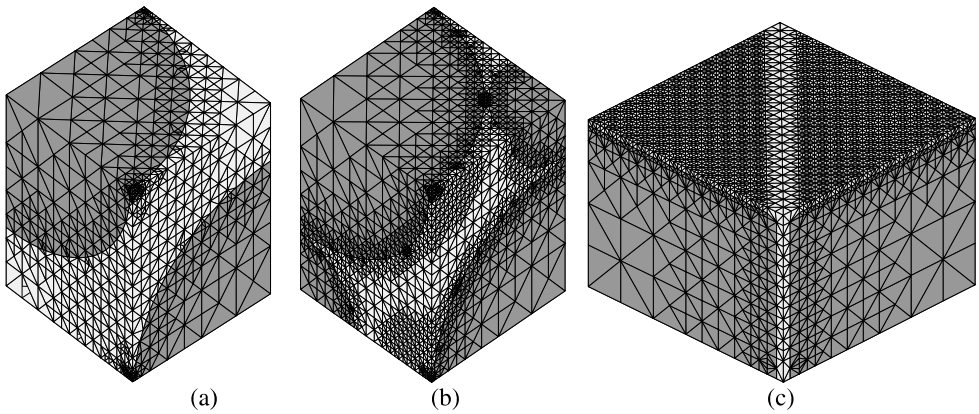

Fig. 3. Reduced unit cell meshes for variety of particulate reinforced composites with 50% inclusion volume fraction: (a) one-sized spherical reinforcement; (b) two sizes of spherical reinforcement; (c) single-sized cubical inclusion.

are linear response, and boundary conditions which do not change from displacement type to load type with time. To predict the effective or macroscopic viscoelastic response of the composite, the real and imaginary parts are separated in the solution, and the results plotted as a stiffness-loss map.

Deviations from this sort of composite theory may arise from mechanisms not accounted for in the theory, which assumes a purely mechanical apposition of the constituents. For example, residual stresses due to differential shrinkage as cast composites are cooled can generate dislocations in the metal matrix. These dislocations can give the matrix material higher damping than it would feature in pure cast form. Thermoelastic effects involving heat transfer among composite constituents can also contribute to the damping of composites as well as in objects such as bent bars, in which the strain field is heterogeneous. Such effects are not accounted for in the purely mechanical composite theory presented above in Section 2.1.

Computed shear modulus versus volume fraction data were subjected to curve fitting following Eq. (3.2) as discussed below in Section 3.2. To obtain viscoelastic properties, the dynamic elastic–viscoelastic correspondence principle was applied to the analytical curve fit expression. The correspondence principle provides a solution to a viscoelastic boundary value problem, given a solution to the corresponding elastic boundary value problem. As input to the model, $G_1^* = 175.43$ GPa $(1 + 10^{-4}$ i) was chosen to model shear stiffness of silicon carbide with an assumed low-damping behavior. The measured viscoelastic shear properties of indium–tin at frequencies in the vicinity of 1 Hz are captured reasonably well with $G_0^* = 7.5$ GPa $(1 + 0.1$ i).

3. Results

3.1. Computed effective elastic moduli

Due to the symmetry of material arrangements considered in the unit cell analysis, the effective elasticity tensor $\mathbf{C}^*$ shows cubic symmetry for all of the particulate composites considered. Both FCC and BCC particle-arrangements feature anisotropy since the material properties vary with direction even though those in the three principal directions are identical to each other. The elastic moduli used for silicon carbide and indium tin are provided in Table 1. To see the anisotropy associated with the particulate-reinforced composite's effective elastic constants, a plane is defined by polar-coordinates whose normal vector is $\hat{r}$ and whose two in-plane axes are $\hat{s}$, $\hat{t}$. Then, the axes $\hat{s}$, $\hat{t}$ are to be rotated within the plane by an angle θ to make general polar-coordinates $\hat{r}'$, $\hat{s}'$, and $\hat{t}'$ (Fig. 4). Note that $\hat{r}' = \hat{r}$, $\hat{s}' = \hat{s}(\hat{r}, \theta)$ and $\hat{t}' = \hat{t}'(\hat{r}, \theta)$. While Young's modulus E is a function of $\hat{r}$ only so that $E = E(\hat{r}')$, the shear moduli G are a function of $\hat{s}'$, $\hat{t}'$ as well as $\hat{r}'$, so that $G = G(\hat{r}', \hat{s}', \hat{t}')$ or $G(\hat{r}', \theta)$. To make it easy to see the variation of G, the maximum and minimum in-plane shear moduli are defined as:

$$\tilde{G}_{\max}(\hat{r}') = \max_{\theta} G(\hat{r}', \theta) \text{ and } \tilde{G}_{\min}(\hat{r}') = \min_{\theta} G(\hat{r}', \theta). \tag{3.1}$$

The three quantities $E(\hat{r}')$, $\tilde{G}_{\max}(\hat{r}')$ and $\tilde{G}_{\min}(\hat{r}')$ are displayed in Figs. 5 and 6, respectively, for a particulate composite with 50% volume fraction of spherical, single-sized reinforcements, and for a particulate

Table 1
Reference elastic moduli of composite constituents at 1 Hz

	Elastic constants		
	E (GPa)	G (GPa)	v
SiC	400	175	0.14
InSn	20.2	7.5	0.35

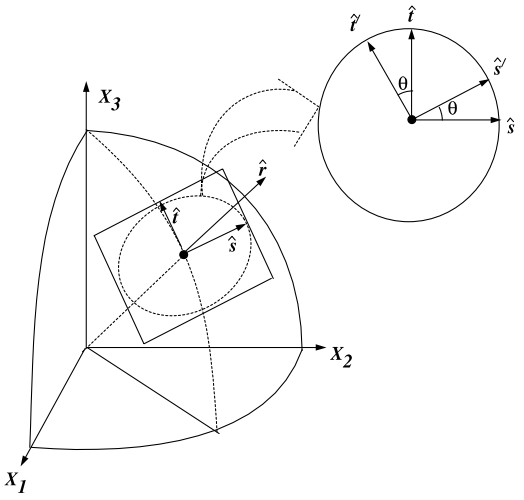

Fig. 4. Polar coordinates $\hat{r}$, $\hat{s}$, $\hat{t}$ and its generalized polar-coordinates $\hat{r}'(=\hat{r})$, $\hat{s}'$, $\hat{t}'$ that are rotated about $\hat{r}$-axis by angle θ: (a) $E(\hat{r}')$; (b) $\tilde{G}_{\max}(\hat{r}')$; (c) $\tilde{G}_{\min}(\hat{r}')$.

composite with 50% volume fraction of cubical, single-sized reinforcements. As can be seen in these figures, E and G reach either their maxima or minima whenever $\hat{r}'$ aligns with the principal axes of the unit cell. The angular variation of G with respect to angle θ in the YZ-plane is presented in Fig. 7 for all three types of particulate composites considered, with each at a reinforcing volume fraction of 50%. The anisotropy associated with the cubical inclusions is clearly greater than that associated with spherical inclusions, either single- or double-sized. Indeed, for the specific cases considered, $E_{\max}/E_{\min} = 1.13$ and $\tilde{G}_{\max}(\hat{r}')/\tilde{G}_{\min}(\hat{r}') = 1.16$ for single-sized spherical inclusions, while $E_{\max}/E_{\min} = 1.6$, and $\tilde{G}_{\max}(\hat{r}')/\tilde{G}_{\min}(\hat{r}') = 1.8$ for cubical inclusions, see Table 2.

For each type of composite considered, the maximum and minimum shear moduli are plotted versus volume fraction in Fig. 8. It is worth noting that for a fixed reinforcement volume fraction, a single-sized spherical inclusion is more effective at increasing shear stiffness than multiple spherical particles of different sizes. However, with multiple sizes of spherical reinforcement, one can ultimately reach higher reinforcement volume fractions, and thus higher effective stiffnesses. With cubically shaped inclusions, using only a single size, it is easier in principle to achieve higher volume fractions of reinforcement than can be achieved using multiple sizes of spherical reinforcement. This is because cubical inclusions, actually fit together when they are arranged in regular patterns. However, to actually manufacture a particulate composite with regular arrangements of cubic inclusions could be quite difficult.

In Fig. 8, results for the cubical structure's lower modulus are lower than the Hashin-Shtrikman lower bound, most notably at the higher volume fractions. That is permissible since the cubic structure exhibits significant anisotropy. The Hashin-Shtrikman formulae represent bounds only in the isotropic case.

3.2. Curve fitting of shear moduli

To facilitate application of the correspondence principle to these particulate composites, the modulus versus volume fraction data have been fitted with analytical expressions. The proposed form is:

$$G = G_0(1 + A_1(\phi - \phi^{A_2}) - \phi^{A_3}) + G_1\phi^{A_4}, \tag{3.2}$$

where the G_0 and G_1 are, respectively, the shear moduli of the matrix and inclusion phases, and A_1, A_2, A_3, A_4 are the free parameters to be estimated. The variable $\phi \in [0, 1]$ is the reinforcement volume fraction. The

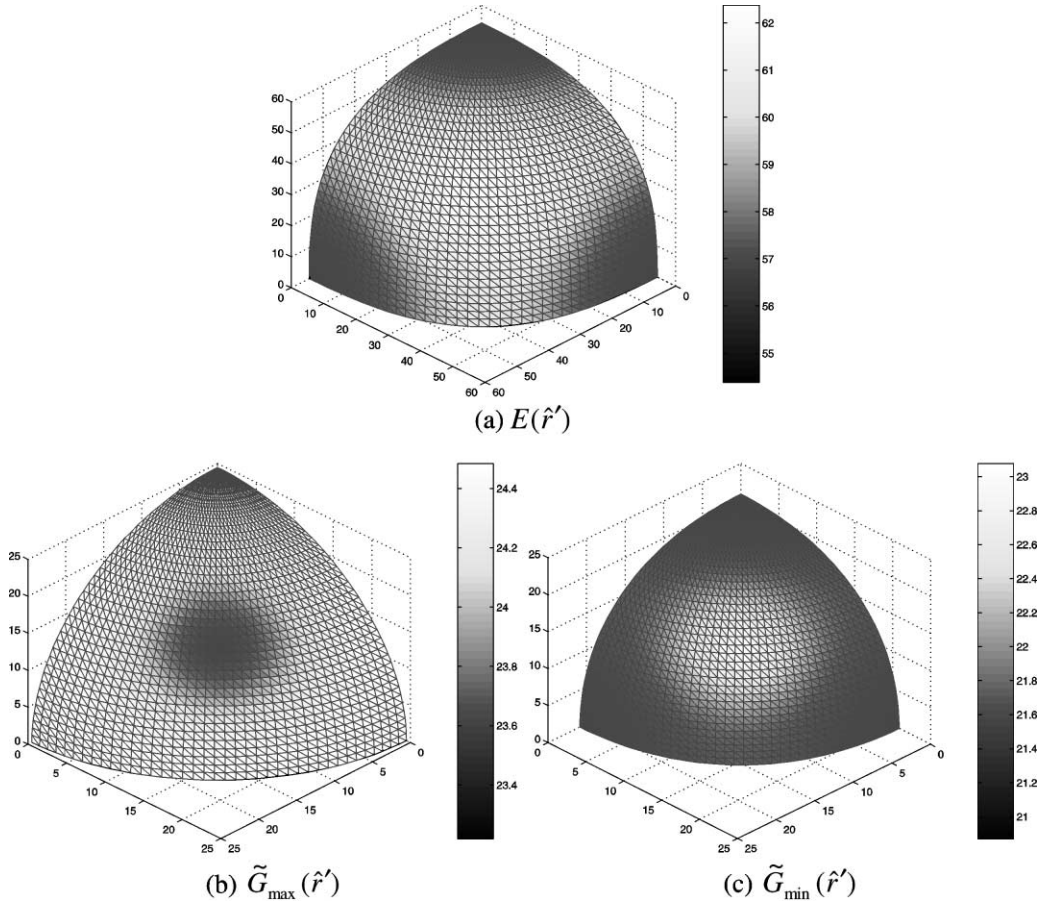

Fig. 5. Variation of Young's modulus and shear modulus with direction $\hat{r}'$ for a composite with 50% volume fraction of spherical SiC reinforcement arranged in FCC pattern: (a) Young's modulus $E(\hat{r}')$; (b) maximum in plane shear modulus $\tilde{G}_{\max}(\hat{r}')$; (c) minimum in plane shear modulus $\tilde{G}_{\min}(\hat{r}')$.

coefficients associated with the best fits to computed moduli for the four different types of particulate-reinforced composites considered are listed in Table 3.

3.3. Viscoelastic behavior: stiffness-loss map

A stiffness-loss map for the various particulate composites, and also for the Hashin-Shtrikman formulae, is shown in Fig. 9. Observe that the Hashin-Shtrikman 'lower' formula, which gives rise to a lower bound of shear modulus for isotropic composites, also gives rise to a lower curve in Fig. 8, modulus versus volume fraction. By contrast, in Fig. 9, the 'lower' formula gives rise to an upper curve, as we have discussed previously (Brodt and Lakes, 1995). The Hashin-Shtrikman formulae enclose a region in the stiffness loss map, but they are in general not bounds. They are usually close to the bounds (Gibiansky and Lakes, 1997). Moreover, properties described by the Hashin-Shtrikman formulae are *exactly attainable* by hierarchical structures, coated spheres (Hashin, 1962) in the case of the bulk modulus, and a hierarchical laminate (Milton, 1986) in the case of the shear modulus.

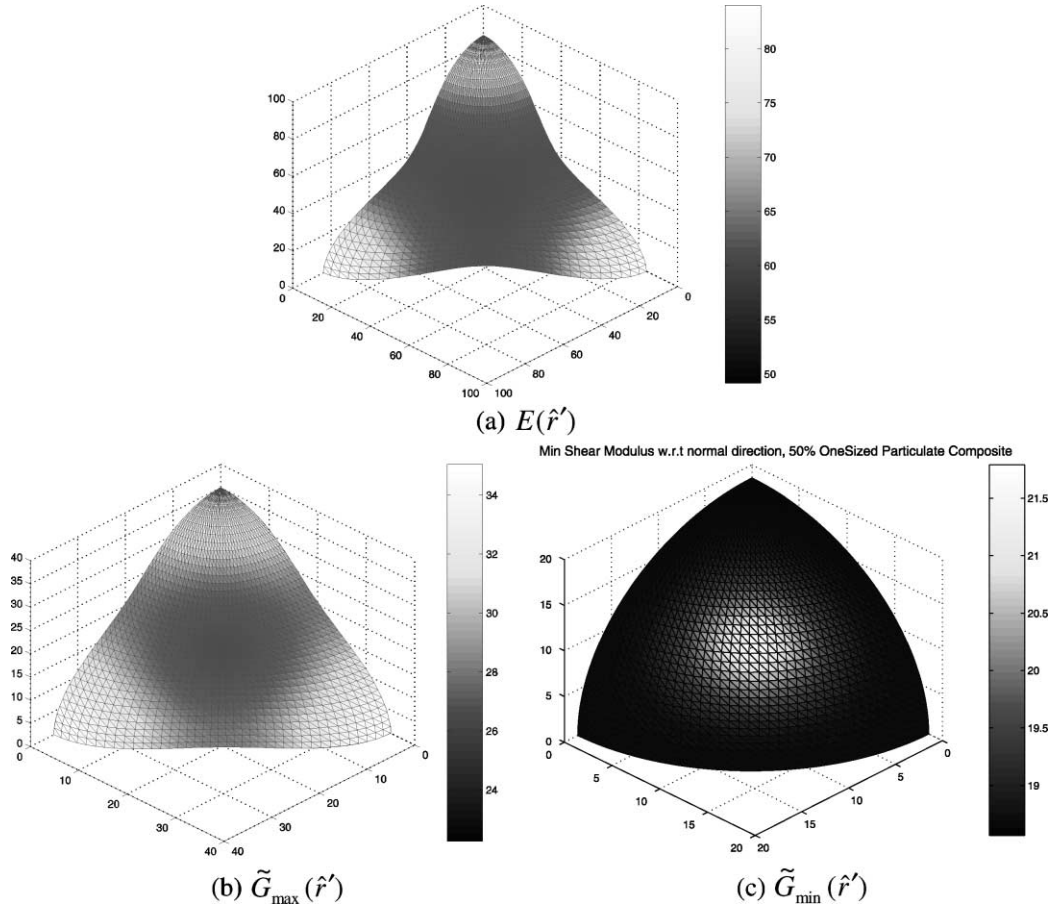

Fig. 6. Variation of Young's modulus and shear modulus with direction $\hat{r}'$ for a particulate composite with 50% volume fraction of cubical SiC reinforcement, arranged in BCC pattern: (a) Young's modulus $E(\hat{r}')$; (b) maximum in plane shear modulus $\tilde{G}_{\max}(\hat{r}')$; (c) minimum in plane shear modulus $\tilde{G}_{\min}(\hat{r}')$.

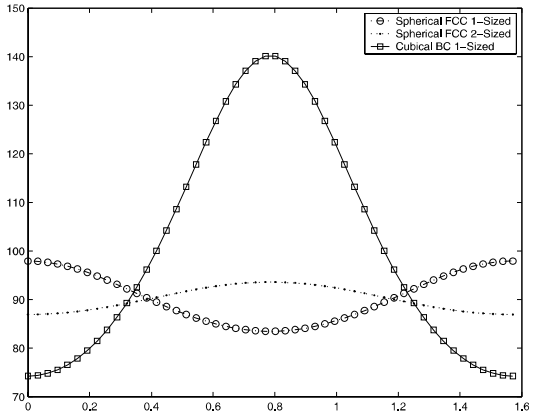

Fig. 7. Variation of shear modulus with respect to angle θ on YZ-plane with three particulate composite model; $\hat{r} = (1, 0, 0)$, $\hat{s} = (0, 1, 0)$, $\hat{t} = (0, 0, 1)$.

Table 2
Variation of homogenized elastic constants with orientation for different particulate-reinforced composites with 50% SiC particle volume fraction

Arrangement/particles	Young's modulus $E(\hat{r}')$		Shear modulus $G(\hat{r}', \theta)$	
	Min	Max	Min	Max
FCC/one-sized spherical particles	54.4	62.4	21.0	24.4
FCC/two-sized particles	56.1	59.8	21.7	23.4
BCC/one-sized cubical particles	49.2	84.0	18.6	35.0

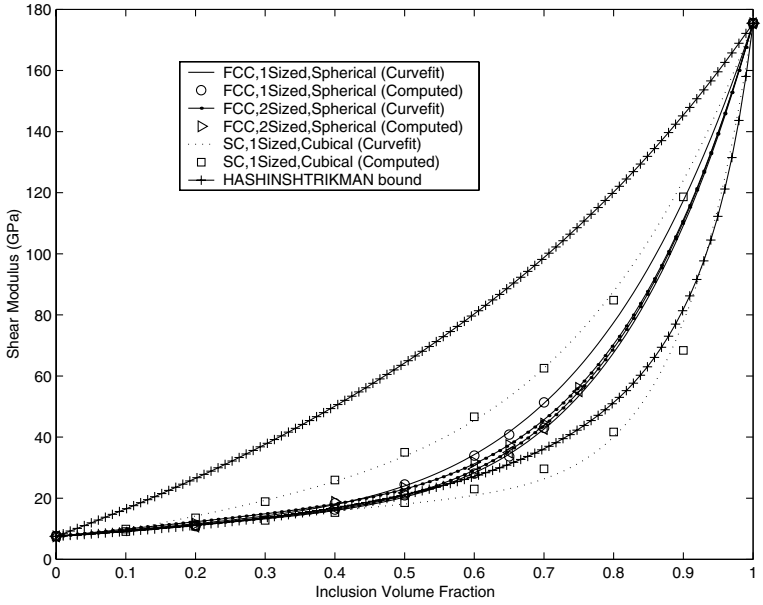

Fig. 8. Computed shear moduli versus volume fractions. Symbols denote discrete computation results and continuous curves denote fits to data points using Eq. (3.2) and the parameters in Table 2. For each composite type, both an upper and lower curve are provided, accounting for directional variations in shear moduli due to anisotropy.

Table 3
Coefficients used to fit shear modulus versus volume fraction results

Type of composite	A_1	A_2	A_3	A_4
FCC single-sized spheres, upper limit	2.698	4.527	4.527	4.527
FCC single-sized spheres, lower limit	2.452	5.340	5.340	5.340
FCC two-sized spheres, upper limit	3.185	5.339	5.339	5.339
FCC two-sized spheres, lower limit	2.522	5.223	5.223	5.223
BCC one-sized cubicles, upper limit	7.172	4.584	0.364	4.584
BCC one-sized cubicles, lower limit	2.789	9.985	9.985	9.985

For the smaller volume fractions of inclusion, beginning at the lower right portion of the diagram in Fig. 9, all the present results are close to the Hashin-Shtrikman 'lower' curve. Such behavior is advantageous for damping layers. These results show that achievement of high concentration of particles via lattices of spherical or cubical morphology results in lower performance than the theoretical maximum. Stiffness and damping behaviors for the spherical morphologies considered are rather similar.

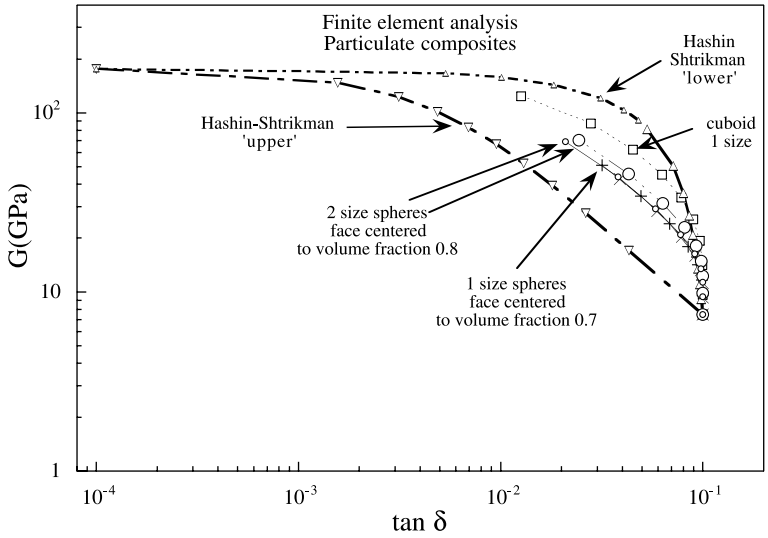

Fig. 9. Stiffness-loss map based on curve fits of shear modulus versus reinforcing volume fraction as shown in Fig. 8. Results are computed for volume fractions in increments of 0.1 up to 0.9 unless otherwise stated. Such high volume fractions cannot actually be attained for the single-sized spherical particle morphologies (see Fig. 8). Upright triangles (△) denote Hashin-Shtrikman upper formulae; inverted triangles (▽), Hashin-Shtrickman lower formula; smaller triangles (△), volume fraction 0.92, 0.94, 0.96, 0.98; squares (□), denote cubical particles, both upper and lower; large open circles (○) denote single-sized spherical particles, both upper and lower; and small open cirles (○) denote multiple-sized spherical particles, both upper and lower.

4. Discussion

The results of this analytical study indicate that material systems of moderately high stiffness and moderately high damping can be achieved using particulate composites having high volume fractions of stiff inclusions embedded in a continuous matrix phase that exhibits high viscoelastic damping characteristics. This study further suggests that cubically shaped inclusions arranged in simple cubic packing arrangements are better for achieving high stiffness and high damping than spherically shaped inclusions. This is because if arranged regularly in simple cubic packing, higher volume fractions of the inclusion material can be obtained with only a single size of inclusion. Furthermore, with cubical inclusions, the composite resembles the Reuss isostress microstructure that forces applied stresses to be channeled through the high-damping matrix phase. Alternatively, with spherical inclusions, one would have to employ a broad spectrum of particle sizes to achieve a high volume fraction.

While the particulate composites with cubical inclusions feature a relatively high degree of anisotropy in both E and G (Figs. 6 and 7), they appear to feature very little anisotropy in $G\tan\delta$ as suggested by the stiffness loss map of Fig. 9. This observation is based on the coincidence of the curves of G versus $\tan\delta$ curves in Fig. 9, based on both $\tilde{G}_{\max}$ and $\tilde{G}_{\min}$ for the composites with cubical inclusions.

Past experience with polymer matrix composites indicates that the peak figure of merit for stiffness and damping, $G\tan\delta$, that can be achieved is typically in the vicinity of 0.23 GPa. With the current class of SiC–InSn composites, the peak figure of merit that can be achieved is 2.7 GPa using cubical inclusions. This represents a substantial improvement. With single-sized spherical inclusions, the present study indicates that $G\tan\delta$ values of 1.6 GPa can be achieved, whereas with two-sized spherical inclusions of SiC embedded in InSn, values of up to 1.7 GPa can be achieved. All of these values assume the stiffness and damping characteristics of InSn at 20 °C and a frequency of 1 Hz.

This study has looked only at the elastic stiffness and viscoelastic damping characteristics of the reinforcing and matrix materials that comprise the composite. In addition, one must also be concerned with the compatibility of the matrix and inclusion materials as measured by their surface energies. A concurrent experimental effort (Ludwigson et al., in press) in which SiC/InSn particulate composites were fabricated and tested indicates that the SiC/InSn surface energy is sufficiently low that molten InSn wets the SiC particles. This is in contrast to the behavior of a pure tin (Sn) matrix which features very poor wetting of SiC.

It is further noted that, the spatial distributions and arrangements of spherical particles have been idealized as periodic. In reality, with existing materials processing techniques, the particle arrangements are more likely to have a strong random component. Dense and random distributions of particle reinforcing could be treated with fairly minor extensions of the current framework. Similarly, the effects of non-spherical particles, and even angular particles could also be treated and quantified in extensions of the current framework.

While some of the assumptions associated with application of the correspondence principle were discussed in Section 2.2, additional discussion is warranted on the modeling details used here. To predict the effective stiffnesses of particulate composites in the neighborhood of 1 Hz for different volume fractions of reinforcement, the reference set of constituent stiffnesses listed in Table 3 were utilized in unit cell analyses. The coefficients listed in Table 2 were obtained by fitting the results of these unit cell analyses to Eq. (3.2) and then used in applying the correspondence principle to obtain the stiffness-loss map of Fig. 9. For frequencies far removed from 1 Hz, different reference viscoelastic constituent stiffnesses would need to be used as input to this process. Since the process employed here is valid strictly for linear viscoelasticity, an alternative approach would be needed (Wu and Ohno, 1999) if non-linear viscoelasticity were involved.

5. Conclusions

Effective stiffness properties of particulate SiC–InSn composites have been computed using unit cell analysis techniques for a wide range of reinforcement volume fractions. The shear modulus versus volume fraction behavior of dilute particulate composites is close to the Hashin-Shtrikman lower bound for single size spherical, two size spherical, and cubical inclusions. For high volume fractions, the shear modulus for all morphologies substantially exceeds the Hashin-Shtrikman lower bound. All of the particulate composites exhibit cubic anisotropy, although the greatest degree of anisotropy occurs with cubical inclusions.

In a stiffness-loss map, the damping behavior of dilute particulate composites is close to the Hashin-Shtrikman 'lower' formula, which gives rise to an upper curve favorable for damping applications. The damping behavior of high volume fraction particulate composites are somewhat was less favorable than that of a Hashin-Shtrikman extremal composite. However, particulate composites with cubical inclusions arranged in simple cubic packing arrangements approach the behavior of the Hashin-Shtrikman extremal composites. In particular, the analytical work of this study suggests that they should be capable of achieving $G\tan\delta$ values of 2.7 GPa, as compared to values of $\approx$0.23 GPa achievable with polymer matrix composites.

Acknowledgements

The authors are grateful for an NSF grant, CMS-9896284, that supported this research.

References

Berlincourt, D.A., Curran, D.R., Jaffe, H., 1964. Piezoelectric and piezomagnetic materials and their function in transducers. In: Mason, E.P. (Ed.), Physical acoustics, vol. 1A, pp. 169–270.

Brodt, M., Lakes, R.S., 1995. Composite materials which exhibit high stiffness and high viscoelastic damping. Journal of Composite Materials 29, 1823–1833.

Buechner, P.M., Stone, D., Lakes, R.S., 1999. Viscoelastic behavior of superplastic 37 wt% Pb 63 wt% Sn over a wide range of frequency and time. Scripta Materialia 41, 561–567.

Christensen, R.M., 1969. Viscoelastic properties of heterogeneous media. Journal of the Mechanics and Physics of Solids 17, 23–41.

Christensen, R.M., 1979. Mechanics of composite materials. John Wiley and Sons, New York.

Dooris, A., Lakes, R.S., Myers, B., Stephens, N., 1999. High damping indium–tin alloys. Mechanics of Time Dependent Materials 3, 305–318.

Dumont, S., Lebon, F., 1996. Wavelet-Galerkin method for periodic heterogeneous media. Computers and Structures 6 (1), 56–65.

Francfort, G.A., Murat, F., 1986. Homogenization and optimal bounds in linear elasticity. Archive for Rational Mechanics and Analysis 94, 307–334.

Gibiansky, L.V., Lakes, R.S., 1997. Bounds on the complex bulk and shear moduli of a two-dimensional two-phase viscoelastic composite. Mechanics of Materials 25, 79–95.

Goodman, G., 1953. Ferroelectric properties of lead metaniobate. Journal of the American Ceramic Society 36, 368–372.

Guedes, J., Kikuchi, N., 1991. Preprocessing and postprocessing for materials based on homogenization method and adaptive finite element methods. Computer Methods in Applied Mechanics and Engineering 83, 143–198.

Hashin, Z., 1962. The elastic moduli of heterogeneous materials. Journal of Applied Mechanics 29, 143–150, Trans. ASME, 84E.

Hashin, Z., 1970. Complex moduli of viscoelastic composites: I. General theory and application to participate composites. International Journal of Solids and Structures 6, 539–552.

Ju, J.W., Chen, T.M., 1994. Effective elastic moduli of two-phase composites containing randomly dispersed spherical inhomogeneities. Acta Mechanica 103, 123–144.

Ju, J.W., Sun, L.Z., 2001. Effective elastoplastic behavior of metal matrix composites containing randomly located aligned spheroidal inhomogeneities Part I: Micromechanics-based formulation. International Journal of Solids and Structures 38 (2), 183–201.

Kim, H.J., Swan, C.C. Voxel based meshing and unit cell analysis of textile composites. International Journal for Numerical Methods in Engineering, in press.

Kim, H.J., Swan, C.C., 2002. Automated meshing and unit cell analysis of periodic composites with hierarchical quadratic tetrahedral elements, in review.

Lakes, R.S., Quackenbush, J., 1996. Viscoelastic behaviour in indium tin alloys over a wide range of frequency and time. Philosophical Magazine Letters 74, 227–232.

Lee, T., Lakes, R.S., 2001. Damping properties of lead metaniobate. IEEE Transactions on Ultrasonics Ferroelectrics and Frequency Control 48 (1), 48–52.

Lloyd, D.J., 1994. Particle reinforced aluminium and magnesium composites. International Materials Reviews 39, 1–23.

Ludwigson, M.N., Swan, C.C., Lakes, R.S. Damping and stiffness of particulate SiC-InSn composite, Journal of Composite Materials, in press.

Michel, J.C., Moulinec, H., Suquet, P., 2001. A computational scheme for linear and non-linear composites with arbitrary phase contrast. International Journal for Numerical Methods in Engineering 52, 139–160.

Milton, G.W., 1986. Modeling the properties of composites by laminates. In: Erickson, J.L., Kinderlehrer, D., Kohn, R., Lions, J.L. (Eds.), Homogenization and effective moduli of materials and media. Springer Verlag, Berlin, pp. 150–175.

Swan, C.C., 1994. Techniques for stress- and strain-controlled homogenization of inelastic periodic composites. Computer Methods in Applied Mechanics and Engineering 117, 249–267.

Swan, C.C., 2001. FENDAC, A finite element code for nonlinear dynamic analysis. Available from <http://www.engineering.uiowa.edu/~swan/software/fendac.pdf>.

Swan, C.C., Kosaka, I., 1997. Homogenization-based analysis and design of composites. Computers and Structures 64 (1–4), 603–621.

Tandon, G.P., Weng, G.J., 1986. Stress distribution in and around spheroidal inclusions and voids at finite concentrations. Journal of Applied Mechanics 53, 511–518.

Wu, X., Ohno, N., 1999. A homogenization theory for time-dependent nonlinear composites with periodic internal structure. International Journal of Solids and Structures 36, 4991–5012.